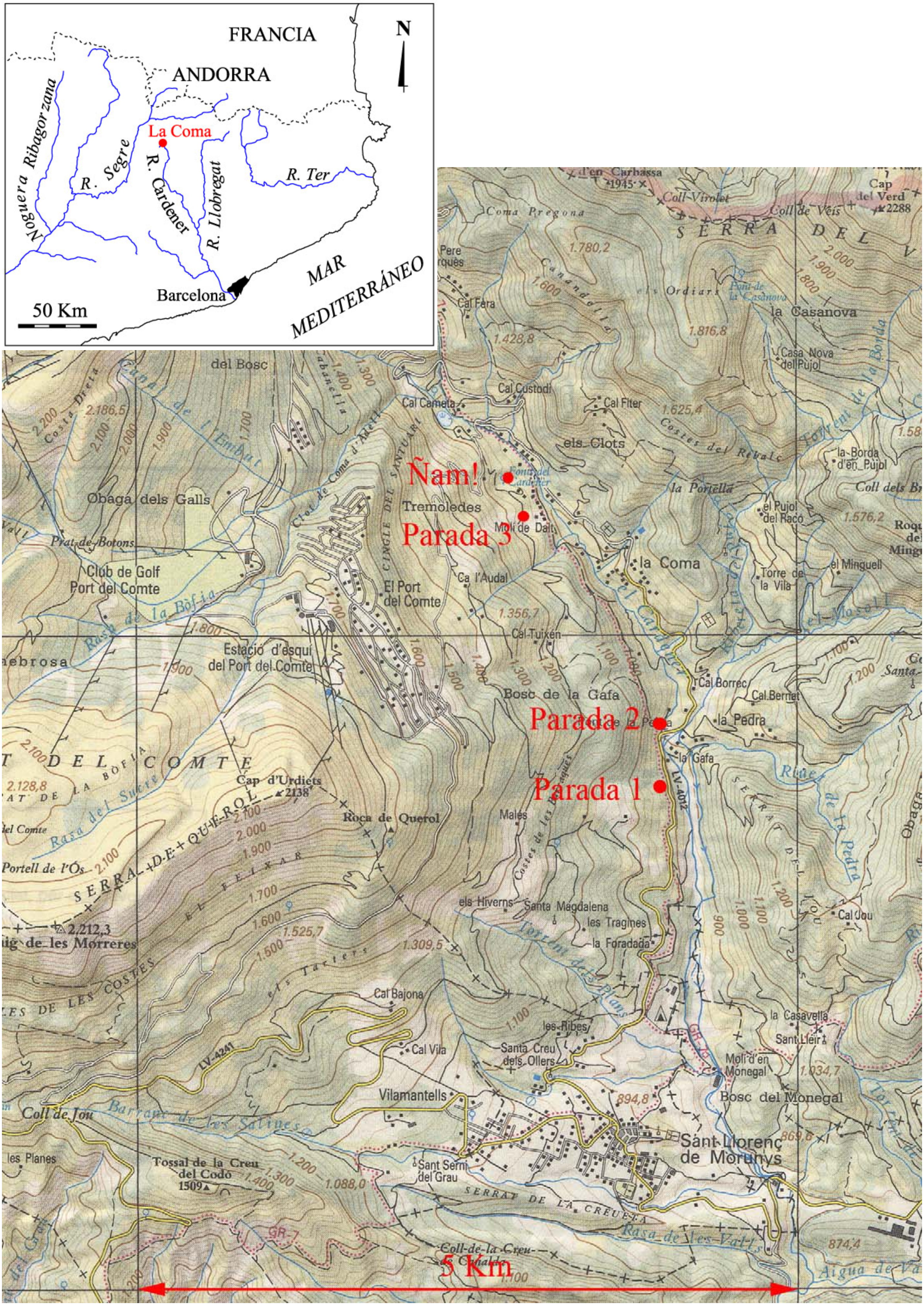
FRANCIA
ANDORRA
N
La Coma
Noguera Ribagorzana
R. Segre
R. Cardener
R. Llobregat
R. Ter
MAR
MEDITERRÁNEO
Barcelona
50 Km
Ñam!
Tremoledes
Parada 3
Parada 2
Parada 1
la Coma
El Port del Comte
Estació d'esquí del Port del Comte
Club de Golf Port del Comte
Obaga dels Galls
Bosc de la Gafa
la Pedra
la Gafa
Roca de Querol
Cap d'Urdiets 2138
Santa Magdalena
les Tragines
la Foradada
els Hiverns
Cal Bajona
Cal Vila
Vilamantells
Santa Creu dels Ollers
les Ribes
Sant Llorenç de Morunys
Bosc del Monegal
Molí d'en Monegal
la Casavella
Sant Lleir
Coll de Jou
les Planes
Tossal de la Creu del Codó 1509
Sant Serni del Grau
la Casanova
els Clots
la Portella
Torre de la Vila
Cal Custodi
Cal Fiter
Cal Cameta
Cal Fera
Coll de Vels
Coll Virolet
Cap del Verd 2288
SERRA DEL V
SERRA DE QUEROL
5 Km

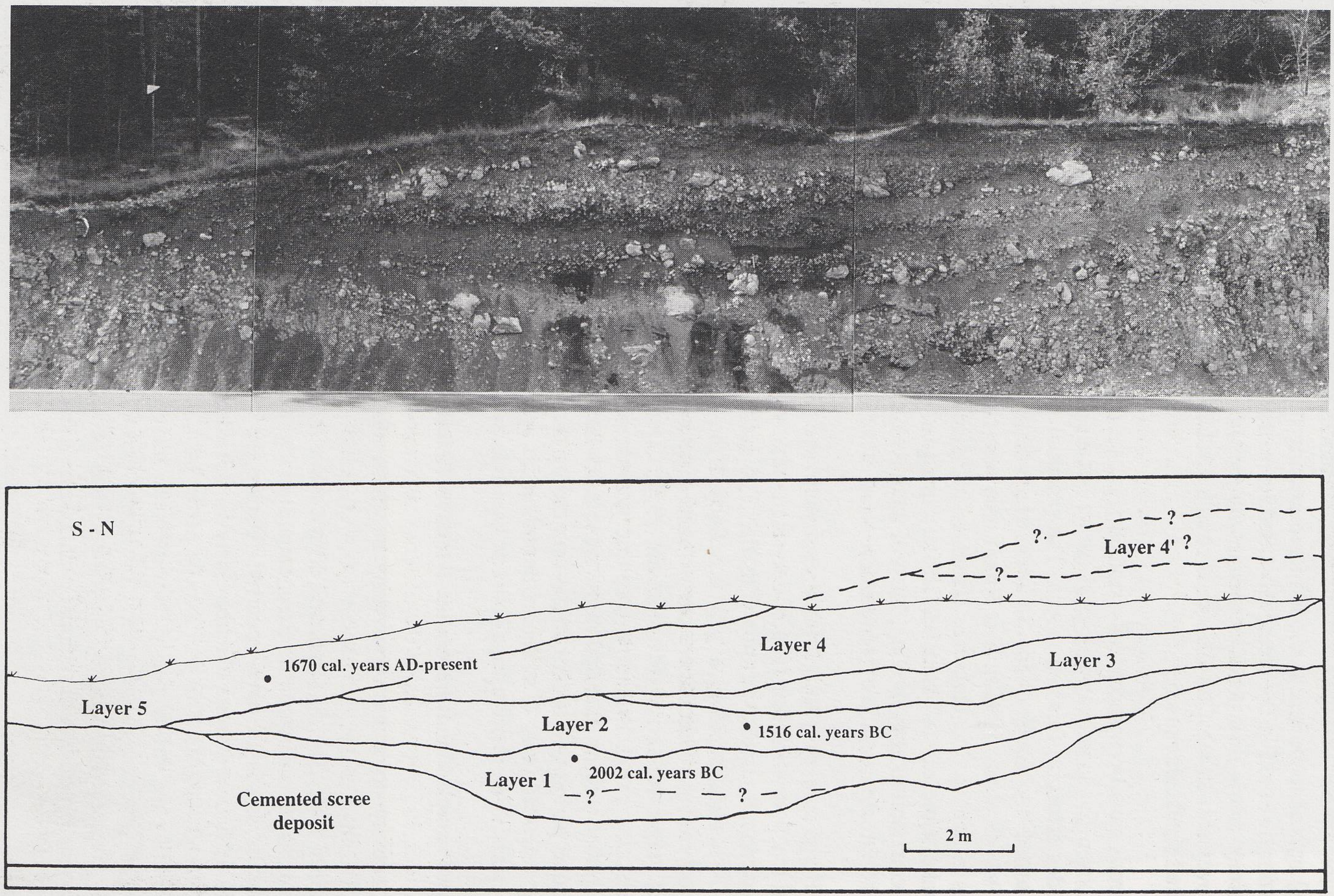

Fig. 7 Location and ages of charcoal samples at the Pedra site. The bases of debris-flow layers are clearly erosive, suggesting that the stratigraphic record may not be complete. Thus, we can suppose that more debris-flow layers were deposited (e.g., layer 4') and afterwards eroded

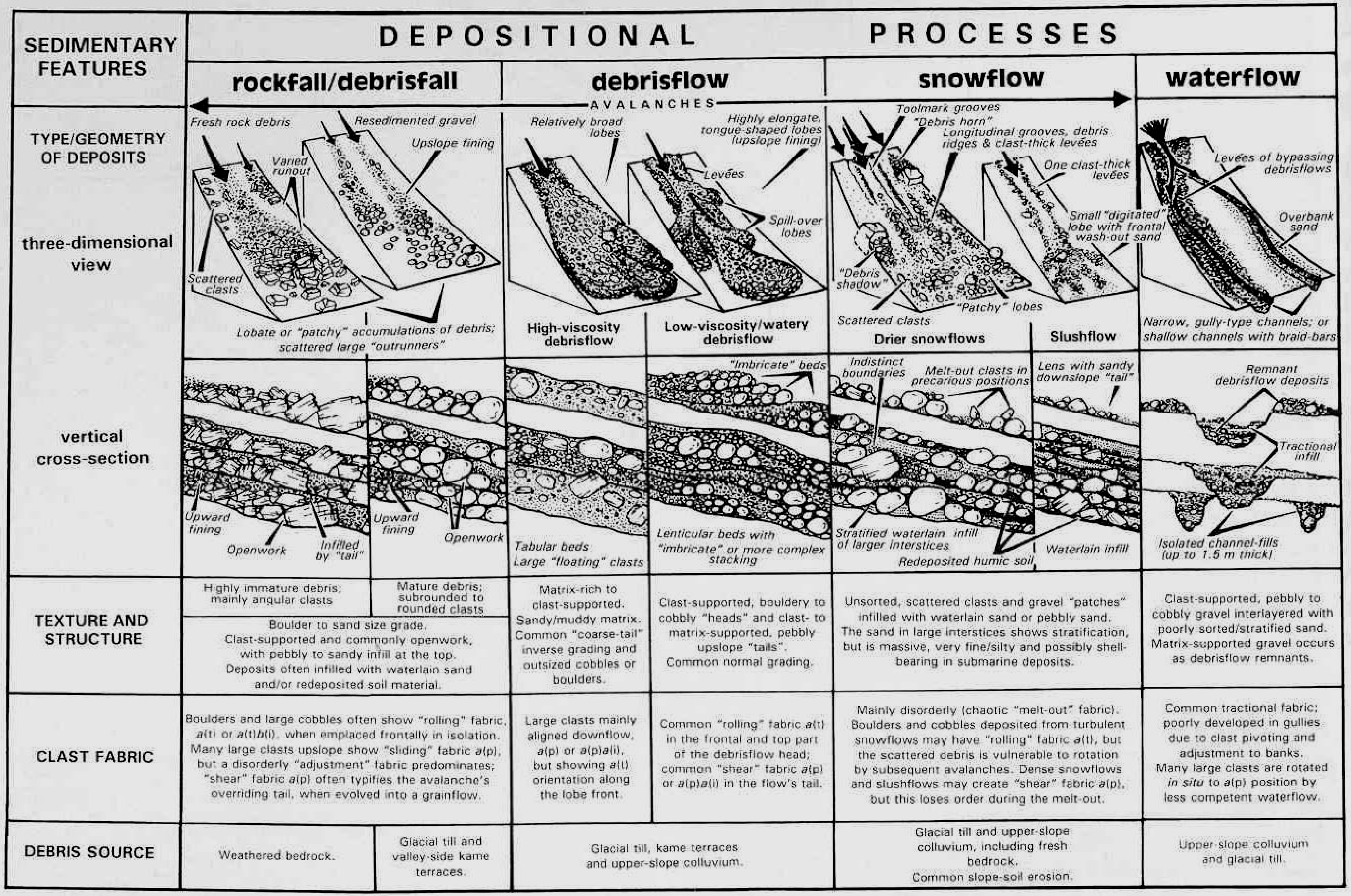

Fig. 6. Summary of the main depositional processes and facies of colluvial fans/aprons, with special reference to the postglacial colluvium in western Norway.

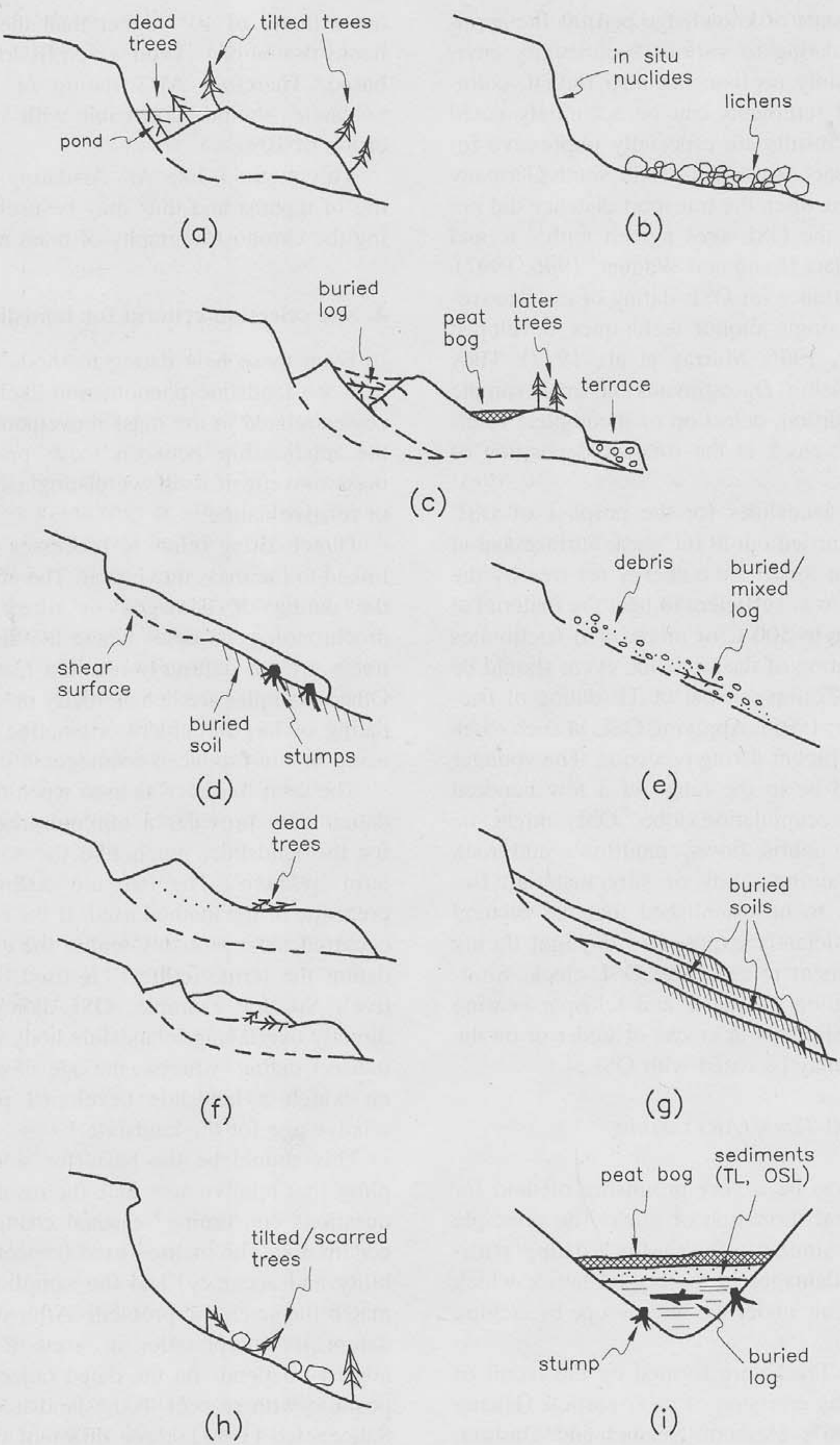

Fig. 3. Location of datable elements relative to the landslide body (see explanations in the text).

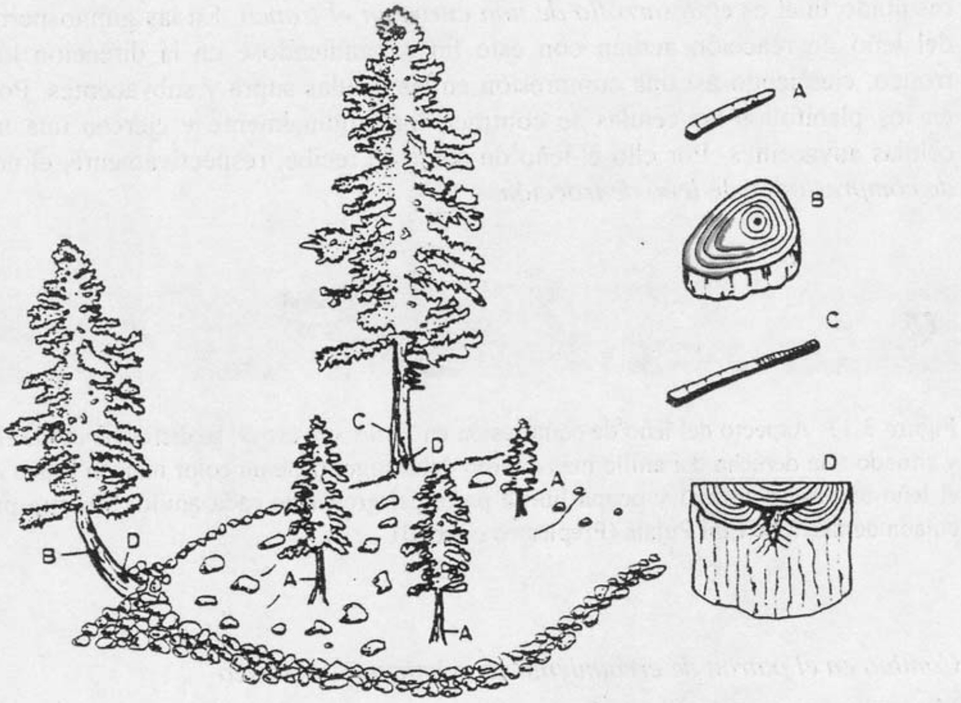

Figura 3.12. Criterios dendrogeomorfológicos para la datación de un movimiento de ladera: a) colonización de la nueva superficie del terreno, estos árboles proporcionan la edad mínima del movimiento; b) crecimiento con leño de reacción (en color más oscuro) y excéntrico (en árboles inclinados); c) aumento de la tasa de crecimiento por eliminación de árboles competidores; y d) herida causada por la erosión (asociada, por ejemplo, a una corriente de derrubios) o al impacto de un bloque (modificada de Osterkamp y Hupp, 1987).

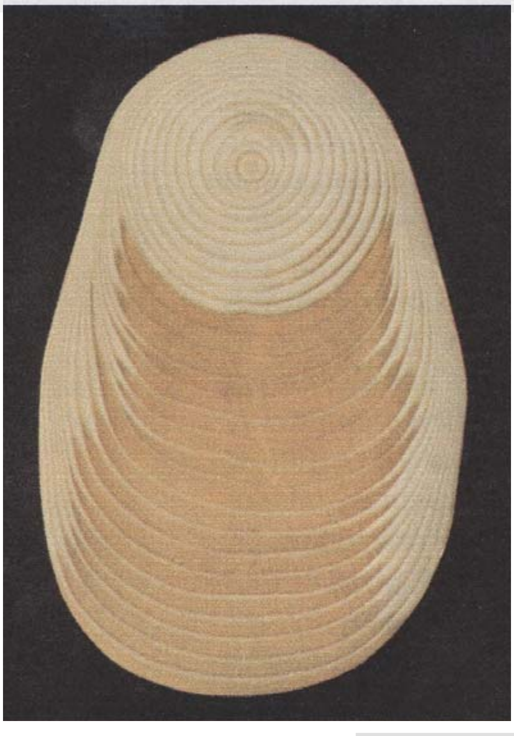

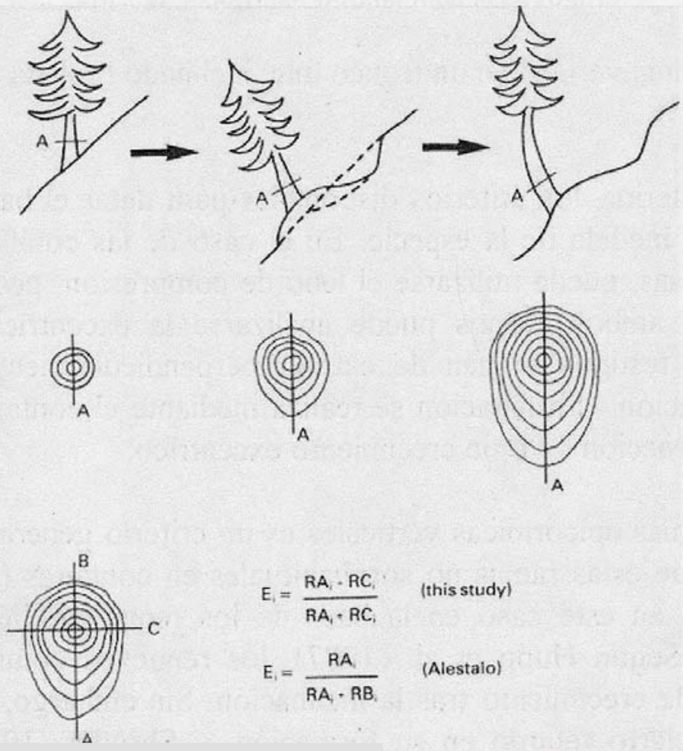

Figura 4.1. Sección transversal de una conífera inclinada. Puede distinguirse claramente el crecimiento concéntrico en los primeros anillos y el posterior crecimiento excéntrico y con leño de compresión (Timell, 1986).

Figura 3.15. Orientación de las muestras para el cálculo de la excentricidad, según Alestalo (1971) y según Braam et al. (1987a) (extraída de Braam et al., 1987a).

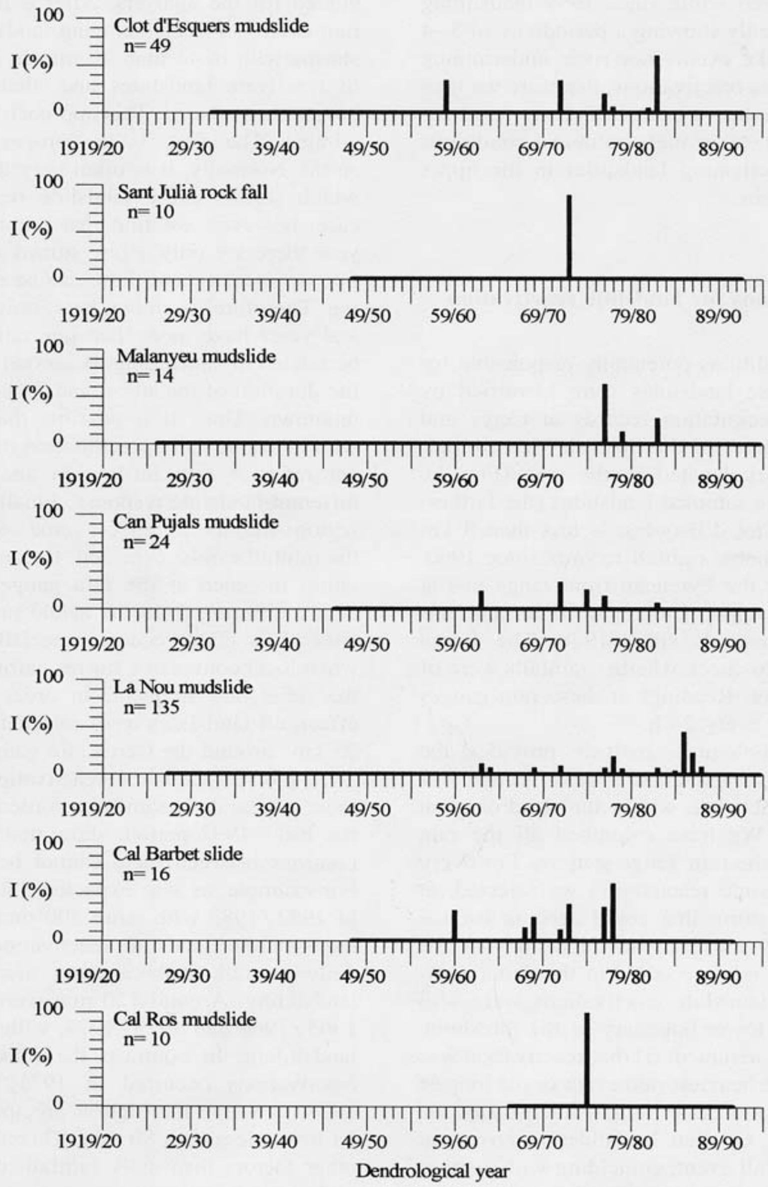

Fig. 4. Landslide reactivations deduced by dendrogeomorphological analysis at the seven landslide sites sampled at the upper Llobregat River basin. *I*: activity index (percentage of trees showing tree-ring response to landsliding); *n*: number of sampled trees; thick solid line indicates the span of time covered by the sampled trees.

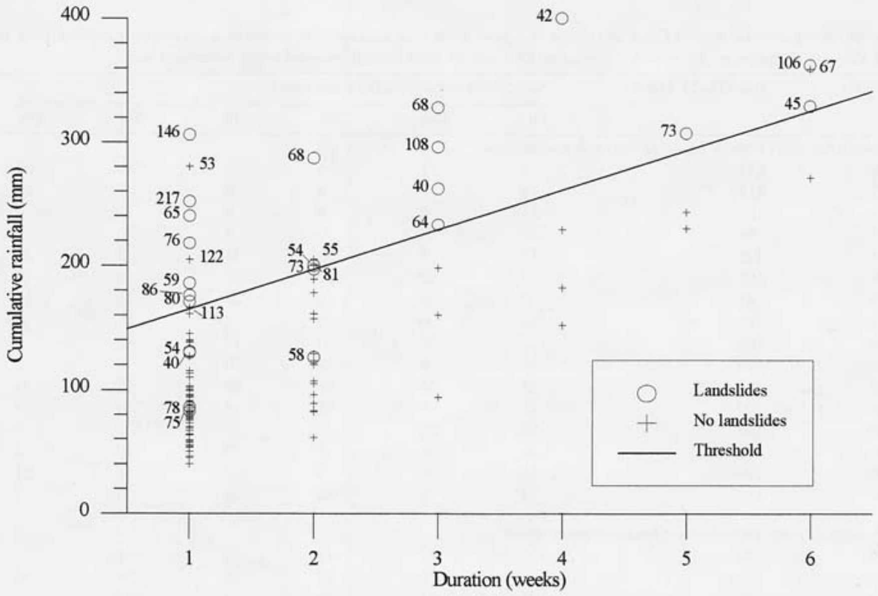

Fig. 7. Cumulative rainfall-duration threshold for reactivation of landslides in the upper Llobregat river basin obtained from all the events with a daily rainfall total greater than 40 mm. Precipitation recorded during the last day of the rain event is indicated in the plot for all the rains associated with landsliding and for those located above the threshold line.

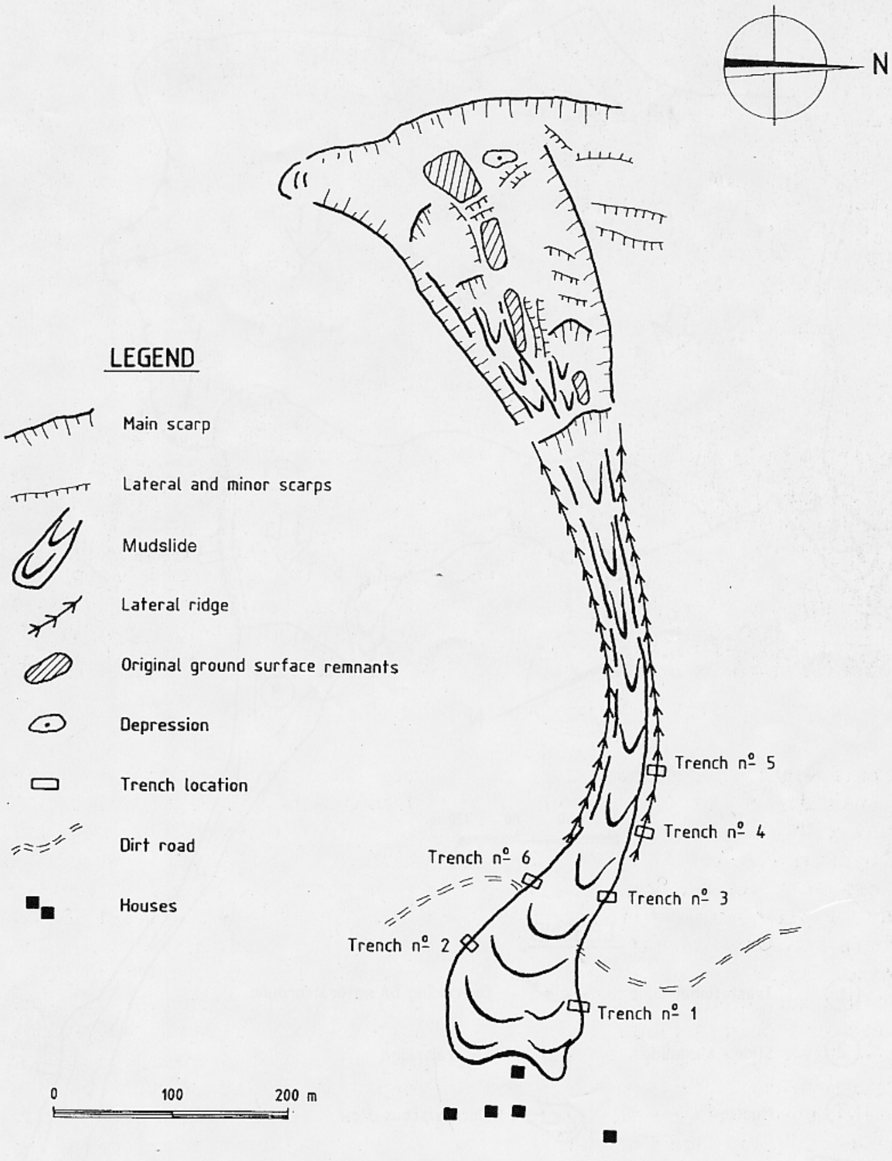

Fig. 10. Map of the La Coma mudslide showing the location of the trenches and some morphological features (modified from Corominas and Moreno, 1988).

Fig. 15. Partial view of trench 5 at the La Coma mudslide. Undisturbed natural ground (*a*) is visible below the outer edge of the ridge; then the contact becomes a steeply dipping shear surface to the left (*b*). An adjacent ridge (*r*), deposited during a second surge of the flow is backed against clasts without matrix (*c*) on top of the first surge. The lateral shear surface (*b*) extends more than 2 m below the original ground surface.

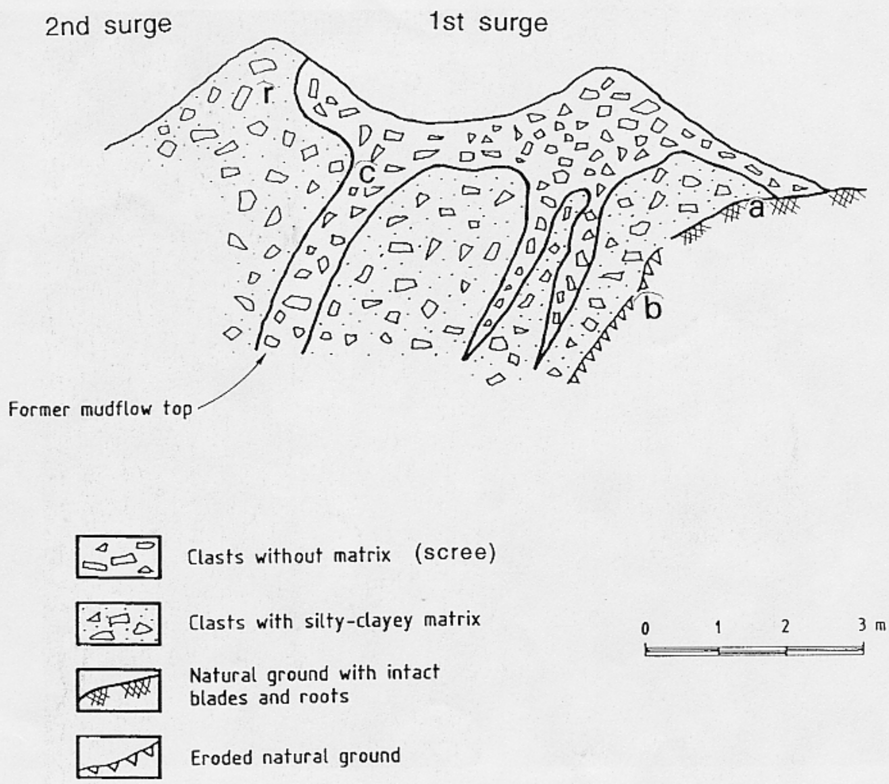

Fig. 16. Cross-section of trench 5 of the La Coma mudslide. The two adjacent lateral ridges were formed during two surges; the main body of the flow is to the left (from Corominas and Moreno 1988). (*a*, *b*, *c* and *r* are the points described in Fig. 15.) The clasts without matrix are scree deposit that were covering the original slope surface at the mudslide head.

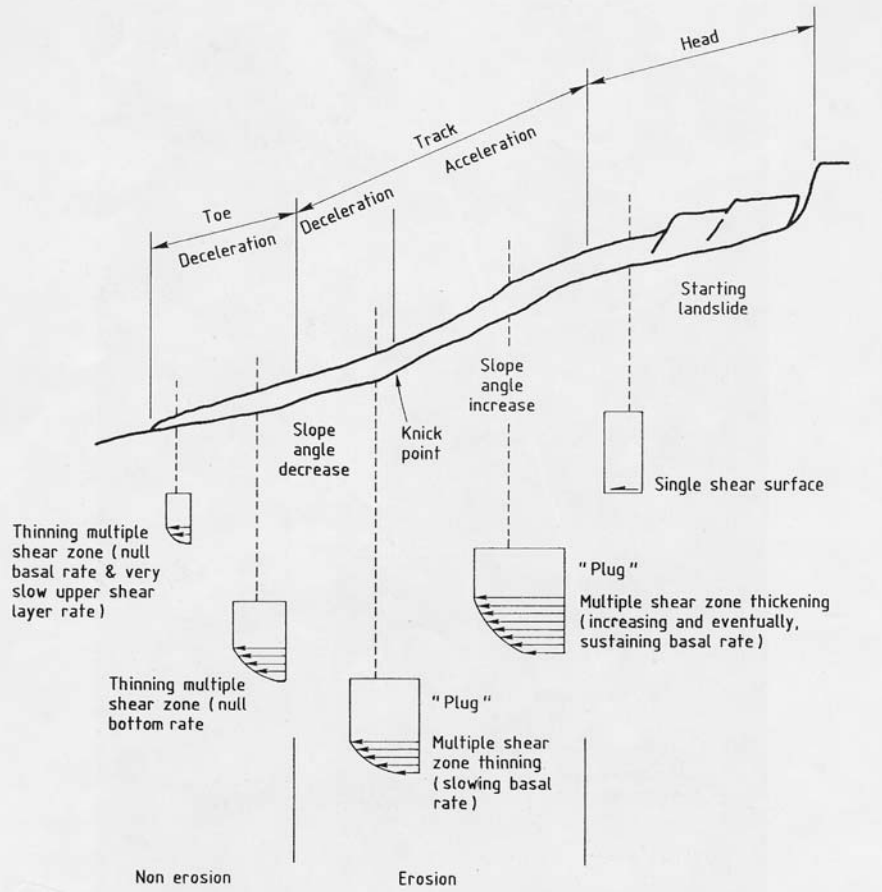

Fig. 23. Idealized velocity distribution along the shear surfaces in a mudslide.

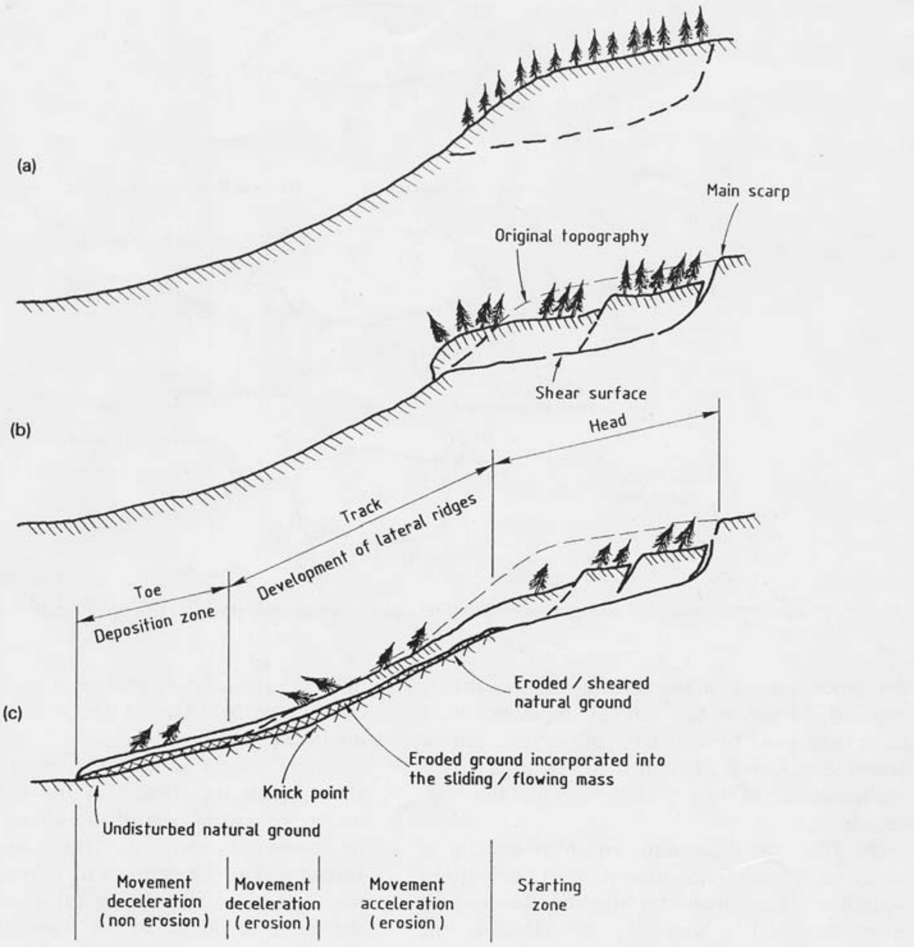

Fig. 24. Location of the ridge development zone on an idealized mudslide or earthflow, considering exclusively the effect of subsidence by ground shearing or erosion.

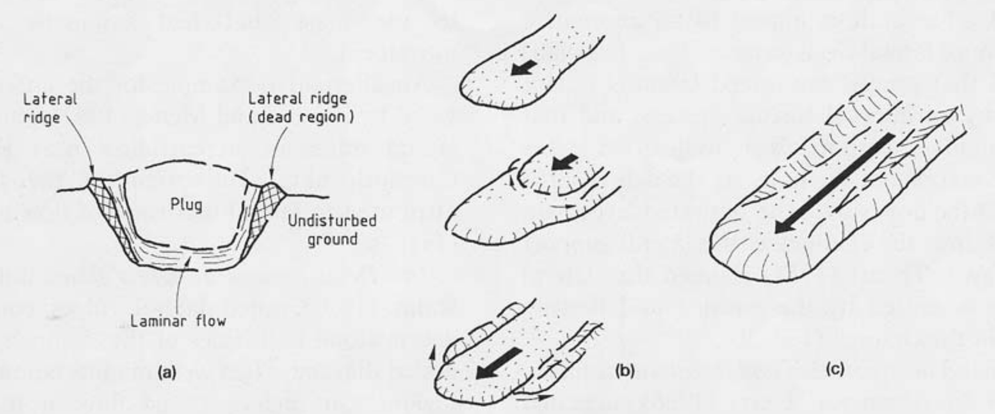

Fig. 4. Suggested mechanisms of lateral ridge development. (a) Lateral ridges as a "dead regions" of flow (Johnson and Rahn, 1970). (b) Overriding of former flows (Keefer and Johnson, 1983). (c) Subsidence of debris surface by diminishing of debris discharge (Johnson and Rodine, 1984). (b) and (c) are interpretive drawings based on descriptions and suggested mechanisms in the above references.

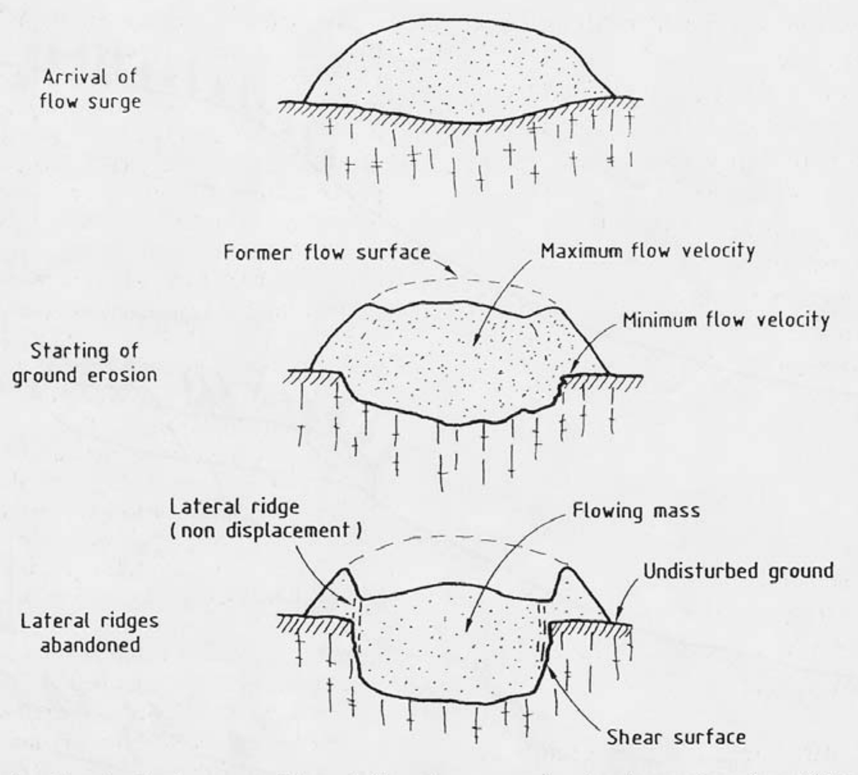

Fig. 25. Cross-section showing the development of lateral ridges by progressive shearing and erosion of the underlying materials.